

MASTER'S PROJECT THESIS
(MAY, 2018-MARCH, 2019)

A novel algorithm based on the principles of diffuse optics to reconstruct the location of optical properties in human tissue



submitted by:

Sumana Chetia

Reg. No.: 20141064, BS-MS Fifth Year

Dept. of Physics

Indian Institute of Science Education and Research (IISER) Pune
India

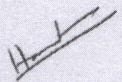
Supervisor:

Dr. Hari M. Varma

Dept. of Biosciences and Bioengineering
Indian Institute of Technology (IIT) Bombay
India

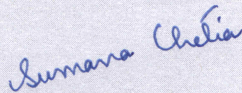
Certificate

This is to certify that this dissertation entitled "A novel algorithm based on the principles of diffuse optics to reconstruct the location of optical properties in human tissue" towards the partial fulfilment of the BS-MS dual degree programme at the Indian Institute of Science Education and Research (IISER), Pune represents study/work carried out by Sumana Chetia at Indian Institute of Technology(IIT), Bombay, India, under the supervision of Dr. Hari M. Varma, Assistant Professor, Dept. of Biosciences and Bioengineering, during the academic year 2018-2019.



(Prof. Hari M. Varma)

Date: 20/03/2019

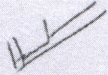


(Sumana Chetia)

Date: 20/03/2019

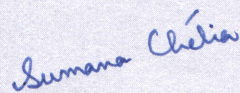
Declaration

I hereby declare that the matter embodied in the report entitled "A novel algorithm based on the principles of diffuse optics to reconstruct the location of optical properties in human tissue" are the results of the work carried out by me at the Department of Biosciences and Bioengineering, Indian Institute of Technology (IIT) Bombay, under the supervision of Prof. Hari M. Varma and the same has not been submitted elsewhere for any other degree.



(Prof. Hari M. Varma)

Date: 20/03/2019



(Sumana Chetia)

Date: 20/03/2019

Acknowledgements

The study of health issues and diseases has always fascinated me. Works of great scientists, from around the world, in the development of advanced instruments for detection of diseases never failed to amaze me. I always wished to work on such topics since my high-school days. I feel blessed to get the opportunity to work on similar topics. It gives me immense pleasure in presenting my Master's project dissertation entitled, "A novel algorithm based on the principles of diffuse optics to reconstruct the location of optical properties in human tissue". I would like to add a few words of appreciation and gratitude for the people who gave me constant support and guidance throughout my project period.

I have carried out my master's project in the Theoretical and Experimental Bioimaging (TEBI) laboratory in the Dept. of Biosciences and Bioengineering in the Indian Institute of Technology (IIT) Bombay, India, led by Prof. Hari M. Varma. I would like to express my sincere thanks to him for believing in my ability to work in this field and thus, providing me the opportunity to do a project under him. His support, timely suggestion, guidance and encouragement helped me to take a step forward towards my dream of working in this field.

I am also thankful to my mentor, Murali Krishnamoorthy, a PhD student working under Prof. Hari M. Varma in IIT Bombay, for his help and support throughout the project period. This work would not have been possible without his help. I would also like to thank Anjali Raghunathan, Technical Superintendent in the Dept. of Biosciences and Bioengineering in IIT Bombay, for helping me in handling the instruments for the experiments. I am also grateful to my other laboratory members for being there with me all the time.

Although I had always been interested in interdisciplinary biology-physics research, my interest got highly enhanced after I joined for an internship under Prof. Samir Kumar Biswas, Dept. of Physical Sciences, Indian Institute of Science Education and Research (IISER) Mohali, India, in December, 2016. This proved to be a major turning point in my academic life. So, I would like to express my heartiest gratitude to him.

I would also like to add a few words of thanks to Prof. Shouvik Datta and Prof. Seema Sharma of Dept. of Physics in IISER Pune for encouraging me throughout. They always helped me to enhance my interest in my research work.

I would also like to thank my family, especially my parents, for helping and supporting me in each step and showing great interest in my work. It would have not been possible for me to carry out my work without their love and support.

Lastly, but not the least, I also thank all my friends for helping me and being with me. I would especially like to thank my roommate, Sanyukta Deshpande, for her motivational discussions with me and helping me to focus on my work in a better way. I am also really grateful to my close friends Rasika Daware, Samikshakiran Agham, Deepshikha, Vrushali Sarwan, Shubhalakshmi Bhat and Megha Chougule for their support throughout.

Sumana Chetia

(Sumana Chetia)

Date: 20/03/2019

Contents

1	Introduction	10
2	Methods	13
2.1	Theory	13
2.1.1	Modeling transfer of photons through tissue	13
2.1.2	Proposed Method: A novel algorithm based on the principles of diffuse optics to reconstruct the location of optical properties in human tissue	18
2.2	Simulations	20
2.2.1	Finite Element Method (FEM)	20
2.2.2	Combination of Jacobians	21
2.3	Experiment	22
2.3.1	Details of the Experimental Components	22
2.3.2	Preparation of Tissue Mimicking Phantoms	24
2.3.3	Experimental Setup	25
3	Results and Discussion	26
3.1	Results	26
3.1.1	Simulation Results	26
3.1.2	Experimental Results	31
3.2	Discussion	33
4	Conclusions and Outlook	33
A	Appendix I : Important Definitions	35
	References	37

List of Figures

1	Laser source directed towards a biological sample (palm of hand).	10
2	The fluence rate versus distance from the source, where the source is considered at the origin.	11
3	The two geometries of source-detector position- (a) reflection geometry and (b) transmission geometry.	12
4	A schematic showing forward model.	15
5	A schematic showing inverse model.	15
6	A schematic showing the Ω and $\partial\Omega$ domains in a sample.	17
7	Experimental setup for the proposed Jacobian combination method.	18
8	The combination of measurements to obtain a square matrix.	19
9	A mesh used for calculations using the Finite Element Method (FEM).	21
10	The Jacobian plotted for a particular pair of source and detector.	21
11	Two Jacobians for two different source-detector pairs in the sample; the most sensitive region as shown by the product of these two Jacobians.	22
12	The laser diode and its set consisting of the current and temperature controllers, the diode mount and the necessary accessories. © <i>Thorlabs</i> [1]	22
13	The beam shaping optical components used in the experiment - a) Collimator , b) Focusing lens and c) Anamorphic Prism Pair. © <i>Thorlabs</i> [1]	23
14	The Galvo mirror used to set the direction of the beam.© <i>Thorlabs</i> [1]	23
15	Laser source directed towards a tissue mimicking phantom which shows similar absorption and scattering properties as biological samples.	24
16	The solid phantom prepared for the experiment and its schematic diagram.	24
17	The CCD camera from Basler used as detector.© <i>Basler</i> [2]	24
18	The setup for the experiment - (a) the schematic diagram and (b) the photograph of the setup.	25
19	The experimental arrangements for taking the measurements in the phantom.	26
20	(a) The FEM mesh of side 3.8cm x 2.3 cm used for the simulations ; (b) the inhomogeneity in absorption coefficient introduced in the mesh.	26
21	The matrix showing the values of the product of measurements due to the two sources for the sample with inhomogeneity.	27
22	The matrix showing the values of the product of measurements due to the two sources for the baseline.	27
23	(a)The matrix showing the percentage change in values of the matrix with respect to the baseline; (b) the position of the inhomogeneity in the sample as shown by the highlighted region; (c) the Jacobian combination showing the detected position of the inhomogeneity.	28

24	A graph showing the given versus the calculated values of μ_a^δ for the inhomogeneity in the sample.	29
25	A graph showing the given versus the calculated values of μ_a^δ for the inhomogeneity in the sample after multiplying the calculated values with the calibration factor.	29
26	(a)The position of the inhomogeneity as shown by the highlighted region;(b) the inhomogeneity reconstructed by inversion of the Jacobian matrix by using Tikhonov regularization.	30
27	(a)The position of the inhomogeneity as shown by the highlighted region;(b) the inhomogeneity reconstructed by using depth compensation algorithm. . . .	30
28	The FEM mesh constructed to plot the Jacobians for the experiment.	31
29	The position of the inhomogeneity as seen by detector arrays located between the source pairs.	32
30	Position of the inhomogeneity as defined by us in the phantom.	32

List of Tables

1	The given and the calculated values of μ_a^δ for the inhomogeneity in the sample.	28
2	The given and the calculated values of μ_a^δ for the inhomogeneity in the sample after multiplying the calculated values by the calibration factor 10.	29
3	The calculated values of μ_a^δ for the inhomogeneity in the experiment after multiplying them by the calibration factor 10.	32

Abstract

In this thesis, we address the problem of reconstructing the optical properties of human tissue from the measured scattered light at the boundary. The conventional methods make the use of Born approximation due to the inherent nonlinear nature of the above-said problem. This involves the inversion of the so-called Jacobian matrix which is always ill-conditioned. Here, we propose a novel algorithm based on the product of several Jacobians corresponding to several measurements which will eventually tell us the location of the optical property without any matrix inversion. In addition, we are also able to recover the value of the optical property along with the location for specific cases. We compare our method against the well-known Tikhonov regularized Born approximation solutions for both simulations and experimental studies.

1 Introduction

Human body is a complex machine. Imaging a human body gives a lot of information to physicians that can assist them in making better decisions. Some existing medical imaging modalities include X-ray, CT scan, MRI, ultrasound, etc. Most of them have radiative sources and are bulky and expensive in nature and this leads to limitations in the usage of such techniques. One of the alternative which is non-invasive and portable is the Near Infrared (NIR) spectroscopy. It is an imaging technique using radiation which lies in the NIR region of the spectrum. In the 1970s, *Jobsis et al* [3] observed high penetration of radiation into biological samples in the NIR region of the spectrum. Better imaging can be obtained if radiation experiences less absorption and high penetration into the medium. So, NIR radiation proved to be a good choice in the entire spectrum of radiation for imaging tissues. Many scientists started using this region of the spectrum for biological imaging purposes[4][5][6][7]. Soon, it started finding great applications in the medical field. It has been used for detection of tumor in breast [8][9][10] as well as in brain [8]. It has also been used for studying the functional activities of different parts of the brain [11][12][13] and thus, address brain-related disorders [14]. Apart from that, it is also used for probing and monitoring flow of blood in patients[15][16][17], and in the study of stroke[18][19].



Figure 1: Laser source directed towards a biological sample (palm of hand).

When light enters a tissue, it starts getting scattered to different directions. This is shown in figure 1, where a laser is directed towards the palm of the hand. It is seen that the laser light no more retains its direction. This is because of the multiple scattering events happening inside the tissue. Apart from that, the intensity (fluence rate) of light is also not preserved throughout its path and it dies off completely after a particular distance. In fact, it is observed that the intensity decreases exponentially with distance as shown in figure 2. This is because of absorption of light by the tissue.

So, tissue has both absorption and scattering properties [20] and these are the major properties that affect the flow of light through the tissue . Thus, there is always an *absorption coefficient* (μ_a) and a *scattering coefficient* (μ_s) and, thereby, their corresponding *absorption length* ($1/\mu_a$) and *scattering length* ($1/\mu_s$) related to the tissue for light of a particular wavelength[21]. Based on the scattering angle due to a single scattering event, the *anisotropy factor* (g) is being defined[20]. In tissues, scattering generally happens in the forward direction with the value of g approximately 0.9 for most cases. By taking the anisotropy factor into consideration, another length scale related to scattering is being considered which is known as *transport mean free path* [21]. This is defined as the distance traveled by light before its direction becomes random. The inverse of the transport mean free path is known as *reduced scattering coefficient* ($\mu'_s = \mu_s(1 - g)$). In general, $\mu'_s \gg \mu_a$ for biological samples [22].

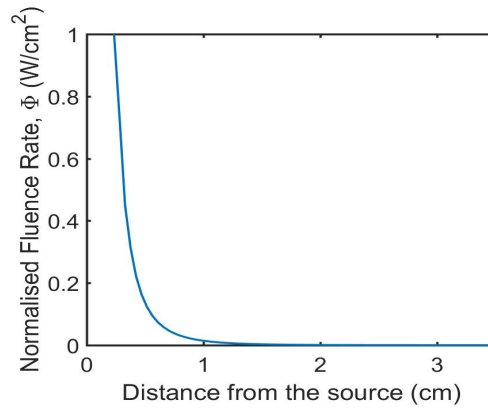


Figure 2: The fluence rate versus distance from the source, where the source is considered at the origin.

Due to high scattering property of tissues, light gets scattered towards all possible directions. As a consequence, when the detector is placed in the same side of the sample as the source, it can detect light. This geometry of placing both source and detector in the same side of the sample is known as *reflection geometry*. For most of the experimental cases, this reflection geometry is being used instead of the *transmission geometry*, where the source and the detector are placed on the opposite sides of the sample. The advantage of using reflection geometry is that it can be used for thicker samples as well, where transmission geometry may not be possible because light may get completely absorbed on its way. Figure 3 shows the two geometries of source-detector positions. The highlighted pink region shows the most probable path of photons inside the sample while traveling from source to detector. These paths are known as *Jacobians* and are defined by the *Jacobian matrix* in the diffusion equation. It is explained in detail in section 2.2.1.

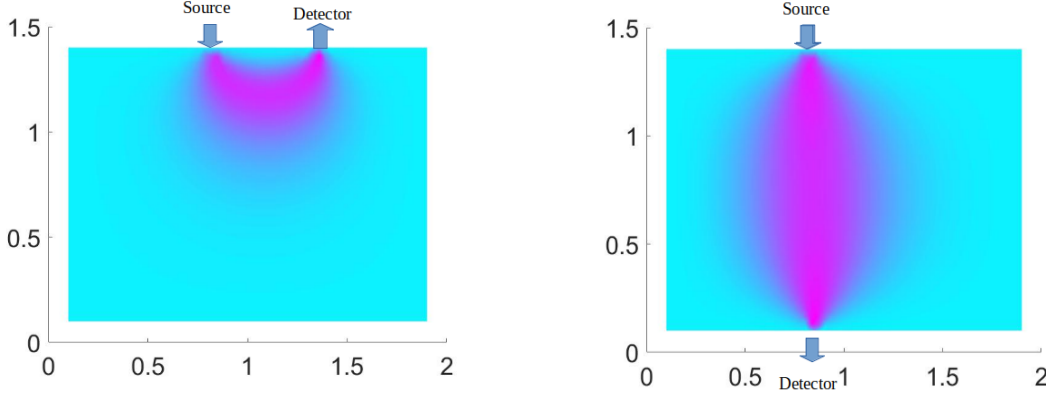


Figure 3: The two geometries of source-detector position- (a) reflection geometry and (b) transmission geometry.

The transfer of photons through a tissue can be mathematically modeled by the *Radiative Transfer Equation* (RTE) [22][23]. This equation basically gives a relation between radiance through the highly scattering medium and the quantitative properties of the medium namely absorption coefficient and scattering coefficient. The main drawback of using this equation directly for study of transfer of photons through a tissue is that this equation is very difficult to solve due to the presence of many independent variables. Due to such complexity of this equation, it is often approximated to average out the variables related to direction and obtain a less complicated form of equation known as the *Diffusion Equation* (DE) [22][24][25]. Imaging, which uses diffusion equation to model transfer of light through the sample, is known as *diffuse optical imaging*.

In an experiment, we generally image a biological sample using diffuse optics to detect the presence of any abnormality or inhomogeneity in the sample. Here, we look for the change in values of the quantitative properties in the inhomogeneity region with respect to the background homogeneous medium. If we have an inhomogeneity in our medium, then by solving the diffusion equation and using the Born approximation (details explained in the section 2.1.1), we can find a relation between the measurement values from our experiment and the perturbation in the tissue properties. This relation is of the form,

$$b = Ax$$

where ‘ x ’ is the matrix containing the unknown perturbation value in the tissue properties, ‘ b ’ is the matrix having the change in measurement values (fluence rate) with respect to the baseline and ‘ A ’ is a matrix that can be calculated which is known as the *Jacobian matrix*. Here, since ‘ x ’ is the unknown matrix, it can be calculated by inverting the matrix ‘ A ’. But this is not directly possible because ‘ A ’ is not a square matrix. So, in most of the cases, it is done using *Tikhonov regularization* method. In this thesis, we present a new way of addressing this problem and detecting the inhomogeneity in the sample without inverting the Jacobian Matrix.

We expect that this can reduce the computational load and give more precise results.

In this thesis, we shall discuss the related theory, the methods implemented by us in the simulations and the experimental setup in the *section 2*. The results obtained from the simulations and the experiments are discussed in *section 3*. A brief conclusion is given in *section 4*. Some important definitions are given in *appendix A*.

2 Methods

2.1 Theory

2.1.1 Modeling transfer of photons through tissue

The *Radiative Transfer Equation* (RTE), which describes the flow of photons inside a highly scattering medium such as a tissue, is given by [22][23],

$$\frac{\partial L(\vec{r}, \hat{s}, t)/c}{\partial t} + \hat{s} \cdot \nabla L(\vec{r}, \hat{s}, t) = -\mu_t(\vec{r})L(\vec{r}, \hat{s}, t) + \mu_s(\vec{r}) \int_{4\pi} (L(\vec{r}, \hat{s}', t)P(\hat{s}', \hat{s}))d\Omega' + S(\vec{r}, \hat{s}, t) \quad (1)$$

where

$L(\vec{r}, \hat{s}, t)$ = radiance at position \vec{r} , traveling in a direction \hat{s} at time t

c = speed of light in vacuum

$\mu_s(\vec{r})$ = scattering coefficient of the medium at position \vec{r}

$\mu_a(\vec{r})$ = absorption coefficient of the medium at position \vec{r}

$\mu_t(\vec{r}) = \mu_s(\vec{r}) + \mu_a(\vec{r})$ = extinction coefficient of the medium at position \vec{r}

$P(\hat{s}', \hat{s})$ = Phase function which gives the probability of light travelling in direction \hat{s}' to get scattered to the direction \hat{s}

Ω' = solid angle in the direction \hat{s}'

$S(\vec{r}, \hat{s}, t)$ = Spatial and temporal distribution of energy from the source at position \vec{r} , traveling in direction \hat{s} at time t

Here, the terms on the left hand side denotes the change in the radiance with respect to time and distance respectively in a particular direction \hat{s} at a particular position \vec{r} in the biological sample. On the other hand, the terms on the right hand side of the equation denotes the properties of the system which leads to this change in the radiance. The first term denotes the contribution by the extinction coefficient leading to loss of radiance in the direction \hat{s} , the second term denotes the scattering from neighboring elements to the element at position \vec{r} and the third terms denotes the contribution by the source directly. The RTE is based on the conservation of energy law for a system containing the incident radiation and the tissue[22]. It can also be derived from the Foldy-Lax formulations[26][27].

The RTE is difficult to solve because it has six independent variables (x, y, z, θ, ϕ, t). So, it is often approximated to the *Diffusion Equation* (DE) [22][24][25] using certain assumptions which is applicable to most of the commonly studied biological tissues. In the diffusion equation, the number of independent variables is four, ie. (x, y, z, t), because here, the radiance is averaged over all directions and thus, the directionality is lost. The assumptions that lead to the diffusion equation are as follows :

(i) *High albedo medium*: The medium is highly scattering and the reduced scattering coefficient is much higher than the absorption coefficient, $\mu'_s \gg \mu_a$.

(ii) *P₁ approximation*: The radiance can be expanded in terms of spherical harmonics to the first order.

(iii) *Fick's Law*: The fractional change in current density \vec{J} within a small length element equal to the transport mean free path ($\frac{1}{\mu'_s}$) is very small (negligible).

(iv) *Isotropic source*: The source is also considered to be isotropic.

These assumptions lead to the introduction of two more terms related to the flow of photons through the medium namely *fluence rate* (Φ) and *current density* (\vec{J}). The definitions are given in appendix A. Thus, using the assumptions, diffusion equation is derived, and is given by:

$$\frac{1}{c} \frac{\partial \Phi(\vec{r}, t)}{\partial t} + \mu_a(\vec{r})\Phi(\vec{r}, t) - \nabla \cdot (D(\vec{r})\nabla\Phi(\vec{r}, t)) = S(\vec{r}, t) \quad (2)$$

where

$\Phi(\vec{r}, t)$ = Fluence rate at position \vec{r} at time t

$D(\vec{r}) = \frac{1}{3(\mu_a(\vec{r}) + \mu'_s(\vec{r}))}$ = Optical Diffusion Coefficient

$S(\vec{r}, t)$ = Spatial distribution of energy from the isotropic source at position \vec{r} at time t

If we are dealing with a continuous source, the diffusion equation for the system will not be time dependent. So, in the time-independent case, it can be written as [22],

$$\mu_a(\vec{r})\Phi(\vec{r}) - \nabla \cdot (D(\vec{r})\nabla\Phi(\vec{r})) = S(\vec{r}) \quad (3)$$

The solution to the equation (3) for a homogeneous infinite medium for a delta source is given by [22]:

$$\Phi(\vec{r}) = \frac{1}{4\pi D(\vec{r})r} \exp(-\mu_{eff}(\vec{r})r) \quad (4)$$

where $\mu_{eff}(\vec{r}) = \sqrt{\frac{\mu_a(\vec{r})}{D(\vec{r})}} = \sqrt{3\mu_a(\vec{r})(\mu_a(\vec{r}) + \mu'_s(\vec{r}))}$ which tells us about the rate at which the fluence rate is decaying spatially.

In practical cases, it is not possible to have an infinite medium. So, the boundary conditions come into picture. We generally consider the medium to be a semi-infinite medium for experimental cases.

In diffusion equation, we come across two problems which are known as the forward model and the inverse model [28]. These are defined below:

Forward Model : When the input and the tissue properties (the absorption and scattering coefficients) are known, and we need to find the output at the boundary by using a given model, then it is known as the forward model. (Figure 4)

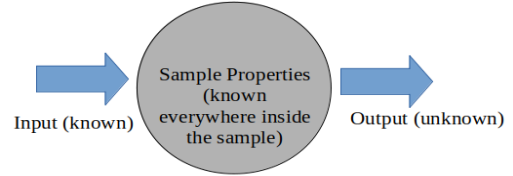


Figure 4: A schematic showing forward model.

Inverse Model : When the input and the output at the boundary are known, and we need to find the tissue properties by using a given model, then it is known as the inverse model. (Figure 5)

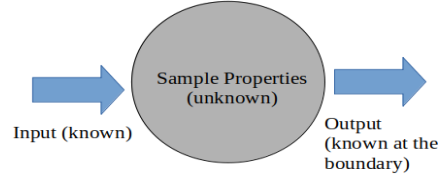


Figure 5: A schematic showing inverse model.

In our experiment, we tried to reconstruct a sample having a inhomogeneity in the absorption coefficient by using the diffusion equation. While doing so, we are always concerned with the change in the properties of the sample due to the presence of the inhomogeneity and not the absolute values of these quantitative properties. This means we are looking for the perturbation in the values instead of the actual values.

Suppose the absorption coefficient is perturbed from $\mu_a(\vec{r})$ to $\mu_a(\vec{r}) + \mu_a^\delta(\vec{r})$. We assume that this changes the fluence rate from $\Phi(\vec{r})$ to $\Phi(\vec{r}) + \Phi^\delta(\vec{r})$. Then, the time independent diffusion equation becomes:

$$(\mu_a(\vec{r}) + \mu_a^\delta(\vec{r}))(\Phi(\vec{r}) + \Phi^\delta(\vec{r})) - \nabla \cdot (D(\vec{r})\nabla(\Phi(\vec{r}) + \Phi^\delta(\vec{r}))) = S(\vec{r}) \quad (5)$$

Subtracting equation (3) from equation (5), we get,

$$\mu_a(\vec{r})\Phi^\delta(\vec{r}) - \nabla \cdot (D(\vec{r})\nabla\Phi^\delta(\vec{r})) = -\mu_a^\delta(\vec{r})(\Phi(\vec{r}) + \Phi^\delta(\vec{r})) \quad (6)$$

Comparing equations (3) and (6), we see that both are almost similar. In equation (6), there is $\Phi^\delta(\vec{r})$ instead of $\Phi(\vec{r})$ and $-\mu_a^\delta(\vec{r})(\Phi(\vec{r}) + \Phi^\delta(\vec{r}))$ instead of $S(\vec{r})$. In equation (3), $S(\vec{r})$ is called the *forcing function* because if there is no source, then this equation will not exist. In the

similar way, in equation (6), $-\mu_a^\delta(\vec{r})(\Phi(\vec{r}) + \Phi^\delta(\vec{r}))$ can be called as the forcing function.

Now, if the source is a delta source, then the solution for equation 3 is called the *Green's function* which is denoted as $G(\vec{r}, \vec{r}')$, where \vec{r} is the position of the observer and \vec{r}' is the position of the source. Any source can be considered as the combination of many point sources. So, for equation (6), if the source is denoted by $-\mu_a^\delta(\vec{r})(\Phi(\vec{r}) + \Phi^\delta(\vec{r}))$, then the solution for this equation is the convolution of Green's functions given as:

$$\Phi^\delta(\vec{r}) = - \int G(\vec{r}, \vec{r}') \mu_a^\delta(\vec{r}') (\Phi(\vec{r}', \vec{r}_s) + \Phi^\delta(\vec{r}', \vec{r}_s)) d\vec{r}' \quad (7)$$

Here, we can see that $\Phi^\delta(\vec{r}', \vec{r}_s)$ is present on both sides and this makes it difficult to solve. So, to simplify this, we use the *Born approximation* which assumes that:

$$\Phi^\delta(\vec{r}', \vec{r}_s) \ll \Phi(\vec{r}', \vec{r}_s)$$

Thus, now in equation 7, we can neglect $\Phi^\delta(\vec{r}', \vec{r}_s)$ in the right hand side under Born approximation and the expression becomes:

$$\Phi^\delta(\vec{r}) = - \int G(\vec{r}, \vec{r}') \mu_a^\delta(\vec{r}') \Phi(\vec{r}', \vec{r}_s) d\vec{r}' \quad (8)$$

This can equivalently be written in the matrix form as

$$\begin{bmatrix} \Phi^\delta(\vec{r}_1) \\ \Phi^\delta(\vec{r}_2) \\ \Phi^\delta(\vec{r}_3) \\ \vdots \\ \vdots \\ \Phi^\delta(\vec{r}_M) \end{bmatrix} = - \begin{bmatrix} G(\vec{r}_1, \vec{r}'_1) \Phi(\vec{r}'_1, \vec{r}_s) d\vec{r}'_1 & G(\vec{r}_1, \vec{r}'_2) \Phi(\vec{r}'_2, \vec{r}_s) d\vec{r}'_2 & \cdot & \cdot & G(\vec{r}_1, \vec{r}'_N) \Phi(\vec{r}'_N, \vec{r}_s) d\vec{r}'_N \\ G(\vec{r}_2, \vec{r}'_1) \Phi(\vec{r}'_1, \vec{r}_s) d\vec{r}'_1 & G(\vec{r}_2, \vec{r}'_2) \Phi(\vec{r}'_2, \vec{r}_s) d\vec{r}'_2 & \cdot & \cdot & G(\vec{r}_2, \vec{r}'_N) \Phi(\vec{r}'_N, \vec{r}_s) d\vec{r}'_N \\ G(\vec{r}_3, \vec{r}'_1) \Phi(\vec{r}'_1, \vec{r}_s) d\vec{r}'_1 & G(\vec{r}_3, \vec{r}'_2) \Phi(\vec{r}'_2, \vec{r}_s) d\vec{r}'_2 & \cdot & \cdot & G(\vec{r}_3, \vec{r}'_N) \Phi(\vec{r}'_N, \vec{r}_s) d\vec{r}'_N \\ \vdots & \vdots & \cdot & \cdot & \vdots \\ \vdots & \vdots & \cdot & \cdot & \vdots \\ G(\vec{r}_M, \vec{r}'_1) \Phi(\vec{r}'_1, \vec{r}_s) d\vec{r}'_1 & G(\vec{r}_M, \vec{r}'_2) \Phi(\vec{r}'_2, \vec{r}_s) d\vec{r}'_2 & \cdot & \cdot & G(\vec{r}_M, \vec{r}'_N) \Phi(\vec{r}'_N, \vec{r}_s) d\vec{r}'_N \end{bmatrix} \begin{bmatrix} \mu_a^\delta(\vec{r}'_1) \\ \mu_a^\delta(\vec{r}'_2) \\ \mu_a^\delta(\vec{r}'_3) \\ \vdots \\ \vdots \\ \mu_a^\delta(\vec{r}'_N) \end{bmatrix} \quad (9)$$

In an experiment, we can obtain the readings for Φ^δ at the boundary of the sample and we need to find the μ_a^δ in all the points in the sample. Thus, equation (9) is of the form,

$$b = Ax \quad (10)$$

Here, 'b' is the matrix consisting of the change in fluence rate (measurement) measured at the detector; 'A' is the matrix consisting of the Green's function terms which is also known as the *Jacobian matrix*; and 'x' is a matrix consisting of the absorption coefficient values at each point in the sample. The matrix 'A' gives the most probable path followed by the photons to reach the detector from the source. Thus, we need to solve for the matrix 'x' to find the properties of the sample in terms of the absorption (and/or scattering) coefficient.

Suppose we consider a sample which can be discretized into ‘N’ nodes (discrete points) inside it (represented as Ω domain) as shown in figure 6. Let ‘M’ be the number of measurements that can be taken in the sample at the boundary (represented as $\partial\Omega$ domain). For all practical cases, $N \gg M$. So, we cannot just invert the matrix ‘A’ to obtain the values of ‘x’ because it is not a square matrix (size of A is $N \times M$). However, a pseudo-inverse can be created to find the values of ‘x’ as shown below [29][30],

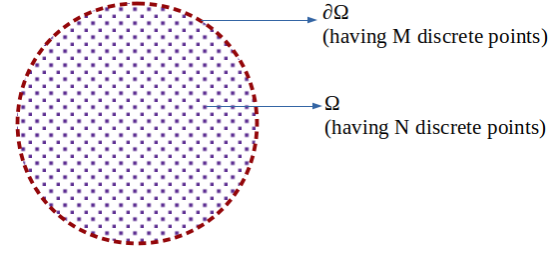


Figure 6: A schematic showing the Ω and $\partial\Omega$ domains in a sample.

$$\begin{aligned}
b &= Ax \\
\Rightarrow A^T b &= A^T Ax \\
\Rightarrow (A^T A)^{-1} A^T b &= (A^T A)^{-1} A^T Ax \\
\Rightarrow (A^T A)^{-1} A^T b &= Ix \\
\Rightarrow x &= (A^T A)^{-1} A^T b
\end{aligned} \tag{11}$$

But this method of finding ‘x’ is very unstable because of the properties of the Jacobian matrix ‘A’. So, instead, it is inverted by the method of *Tikhonov regularization*[29][30]. Using this method, the equation can be written as,

$$x = A^T (AA^T + \lambda_1 \max(\text{diag}(S))I)^{-1} b \tag{12}$$

where λ_1 is a regularization constant and S is the diagonal matrix obtained by Singular Value Decomposition (SVD) of A, ie. $A=USV^T$, where U and V are unitary matrices and S is a rectangular diagonal matrix.

As light passes through a biological sample, its intensity decays exponentially with depth. This results in reduction of sensitivity of measurement values with the increase in depth. So, the reconstructed inhomogeneities are inclined more towards the surface layers. To address this problem, equation (12) was modified to equation (13) [30]. Here, a depth compensation algorithm is embedded in the reconstruction which takes care of the error caused due to reduction of sensitivity with depth.

$$x = (L^{-1}A)^T [(L^{-1}A)(L^{-1}A)^T + \lambda_1 \max(\text{diag}(S))I]^{-1} L^{-1} b \tag{13}$$

where λ_1 is a regularization constant similar to the one in equation (12) and L is a diagonal matrix defined as

$$\text{diag}(L) = [\text{diag}(A^T A) + \lambda_2 \max(\text{diag}(A^T A))]^{1/2}$$

where λ_2 is another regularization constant.

The constants, λ_1 and λ_2 are not easy to find and there is always a possibility of finding better values of these constants and thus, reconstruct the sample in a better way. This enhances the complexity of the problem. In this thesis, we present an alternative way of solving this problem.

2.1.2 Proposed Method: A novel algorithm based on the principles of diffuse optics to reconstruct the location of optical properties in human tissue

We consider two sources and an array of detectors in between them as shown in figure 7. Measurements (fluence rates) are taken from all the detectors.

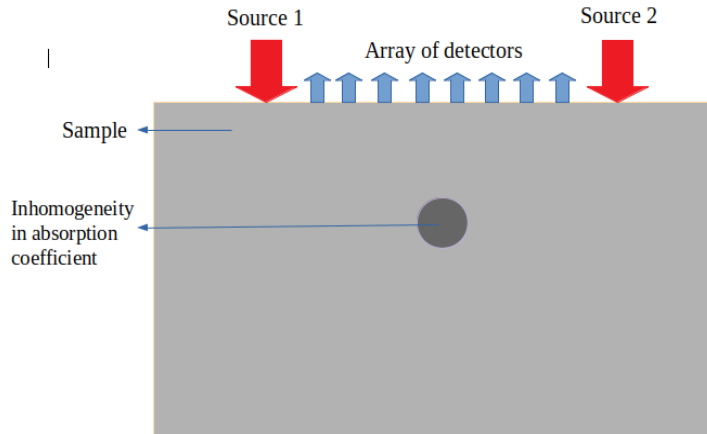


Figure 7: Experimental setup for the proposed Jacobian combination method.

Suppose we label the two sources as source 1 and source 2 respectively as shown in figure 7 and the array of detectors in between them are labelled from left to right. The two sources are switched on individually and the measurements are taken at all the detector positions. These two arrays of measurements are then multiplied to each other such that we can obtain all the combination of measurements corresponding to the two sources. Thus, if we had an array of M detectors between the two sources, then we obtain a $M \times M$ square matrix having all the combinations of measurements as shown in figure 8. (details are explained in section 2.2.2)

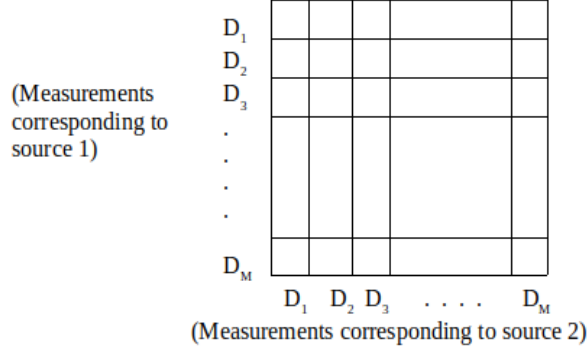


Figure 8: The combination of measurements to obtain a square matrix.

The same process is repeated for the baseline and an $M \times M$ square matrix is obtained for the baseline too. Then, we find the percentage change of each constituent of the matrix with respect to the baseline. It is observed that certain combination of detectors in the matrix shows a very high change compared to the others. So, picking up those detector pairs whose change is higher than a particular threshold value would give us our required source-detector pairs. Plotting the combination (multiplication) of Jacobians for all these pairs would give the position of the inhomogeneity.

For simple cases, we can also find the approximate change in the property of the sample at the position of the inhomogeneity. Let us consider the case where the absorption coefficient is being perturbed at the inhomogeneity region in the sample. Suppose the sample has N nodes (Ω domain) and we consider two pairs of sources and detectors. Let Φ_1^δ and Φ_2^δ be the measurement values at the two detector positions at the boundary of the sample ($\partial\Omega$ domain) due to the two sources. So, in terms of the Jacobian matrix, it can be expressed as

$$\Phi_1^\delta = - \begin{bmatrix} J(\vec{r}_1) & J(\vec{r}_2) & J(\vec{r}_3) & \dots & J(\vec{r}_N) \end{bmatrix} \begin{bmatrix} \mu_a^\delta(\vec{r}_1) \\ \mu_a^\delta(\vec{r}_2) \\ \mu_a^\delta(\vec{r}_3) \\ \vdots \\ \mu_a^\delta(\vec{r}_N) \end{bmatrix} = \sum_{i=1}^N J(\vec{r}_i) \mu_a^\delta(\vec{r}_i) \quad (14)$$

$$\Phi_2^\delta = - \begin{bmatrix} J'(\vec{r}_1) & J'(\vec{r}_2) & J'(\vec{r}_3) & \dots & J'(\vec{r}_N) \end{bmatrix} \begin{bmatrix} \mu_a^\delta(\vec{r}_1) \\ \mu_a^\delta(\vec{r}_2) \\ \mu_a^\delta(\vec{r}_3) \\ \vdots \\ \mu_a^\delta(\vec{r}_N) \end{bmatrix} = \sum_{i=1}^N J'(\vec{r}_i) \mu_a^\delta(\vec{r}_i) \quad (15)$$

Thus, product of the measurement values means taking the product of equations (14) and (15). So, we get

$$\Phi_1^\delta \Phi_2^\delta = \sum_{i=1}^N J(\vec{r}_i) \mu_a^\delta(\vec{r}_i) \sum_{j=1}^N J'(\vec{r}_j) \mu_a^\delta(\vec{r}_j) \quad (16)$$

In the position where the inhomogeneity is present, suppose change in absorption coefficient has a value μ_a^δ . This means, the entire inhomogeneity region has a constant change in absorption coefficient μ_a^δ , and in the rest of the sample it is zero.

Thus, in equation (16), only those values will remain which have both the $\mu_a^\delta(\vec{r})$ non-zero. Suppose, there are p nodes in the sample which has the perturbation in absorption coefficient. Then, equation (16) becomes

$$\Phi_1^\delta \Phi_2^\delta = \left(\sum_{i=1}^p J(\vec{r}_i) \sum_{j=1}^p J'(\vec{r}_j) \right) (\mu_a^\delta)^{2p} \Rightarrow \mu_a^\delta = \left(\frac{\Phi_1^\delta \Phi_2^\delta}{\sum_{i=1}^p J(\vec{r}_i) \sum_{j=1}^p J'(\vec{r}_j)} \right)^{\frac{1}{2p}} \quad (17)$$

So, for a general case, where we consider q detectors for the first source and q detectors for the second source to form the Jacobian combination to detect the position of the inhomogeneity, equation (17) becomes,

$$\mu_a^\delta = \left(\frac{\prod_{i=1}^q \Phi_{1i}^\delta \prod_{j=1}^q \Phi_{2j}^\delta}{\sum_{i=1}^p J(\vec{r}_i) \sum_{j=1}^p J'(\vec{r}_j)} \right)^{\frac{1}{2p}} \quad (18)$$

Thus, for the simple case where the change in absorption coefficient is constant throughout the inhomogeneity region, we can quantify this change. Hence, according to our hypothesis, we can find the approximate location as well as the approximate change in the absorption coefficient by our method for simple cases.

2.2 Simulations

2.2.1 Finite Element Method (FEM)

The simulations are done using the Finite Element Method (FEM) [31][32]. It is a method to solve Partial Differential Equations (PDEs) using appropriate boundary conditions. In this method, the system under consideration is divided into finite number of smaller elements.

Figure 9 shows an FEM mesh of size 1.8cm x 1.3cm which is being subdivided into 4032 elements defined on 2093 nodes. In the simulations, this entire mesh is considered as the sample and calculations are done on it. This mesh is being used for plotting the Jacobians in the section 2.2.2.

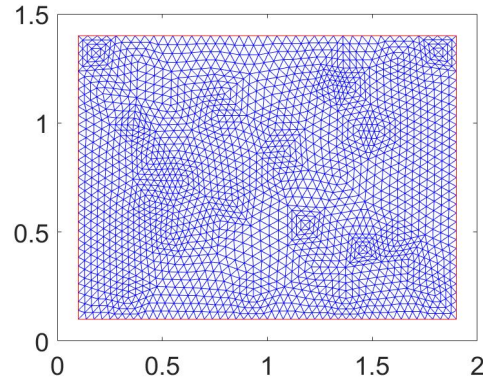


Figure 9: A mesh used for calculations using the Finite Element Method (FEM).

2.2.2 Combination of Jacobians

Suppose we consider a source and a detector placed on the upper surface of the sample represented by the blue region as shown in the figure 10. The red pointer represents the position of the source and the black pointer represents the position of the detector. The most probable path of photons from the source to the detector is given by the Jacobian (highlighted pink region in the figure).

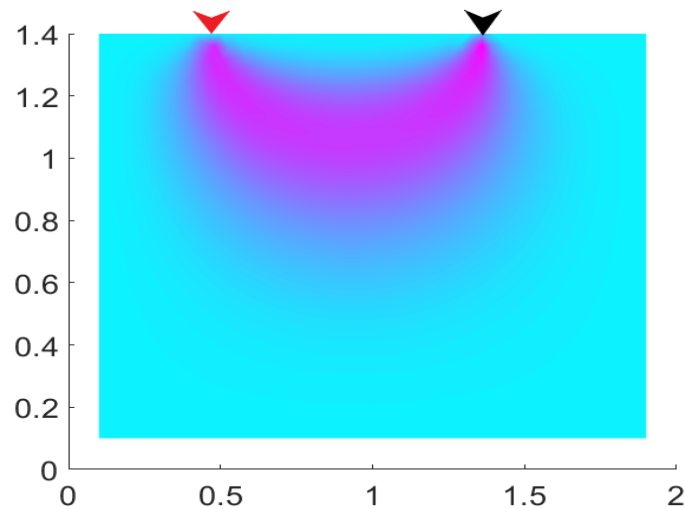


Figure 10: The Jacobian plotted for a particular pair of source and detector.

If we combine (multiply) two such Jacobians for two source-detector pairs, then the region of intersection of the Jacobians is the region which is most sensitive to any change in the properties of the sample. This means if the absorption (and/or scattering) coefficient changes in this region of intersection of the Jacobians, then the product of measurements at those particular detector positions will show the maximum change in its value with respect to the baseline (homogeneous medium).

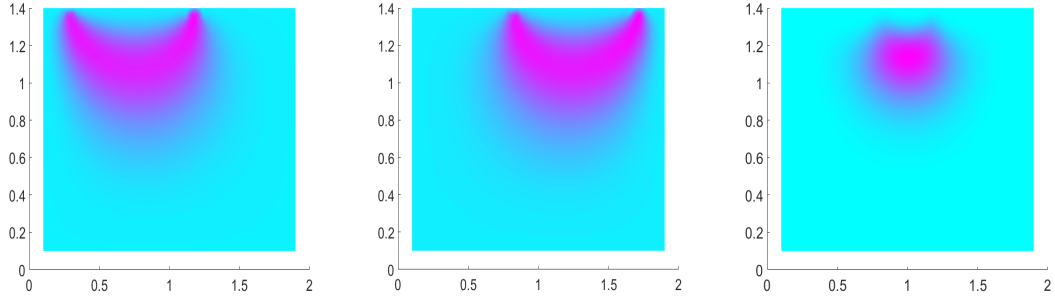


Figure 11: Two Jacobians for two different source-detector pairs in the sample; the most sensitive region as shown by the product of these two Jacobians.

In figure 11 (first two figures), two Jacobians are plotted for two source-detector pairs placed in the upper surface of the sample. When we multiply these two Jacobians, their region of intersection shows a very high sensitivity as shown by the pink highlighted region in figure 11 (last figure). Suppose, the sample has an inhomogeneity in its scattering and/or absorption coefficient at this highlighted region. Then, the product of the fluence rates at the two detector positions will show a high perturbation with respect to the baseline. But, if the inhomogeneity is present in any position other than this highlighted region, then the perturbation in the product of fluence rates at the two detector positions will be almost negligible with respect to the baseline.

We shall be using this concept to locate the position of the inhomogeneity in the sample in our experiments.

2.3 Experiment

2.3.1 Details of the Experimental Components

The experimental setup consists of the following components:

Laser Diode:

The source used in the experiment is a temperature and current controlled laser diode (*Thorlabs, laser diode : L785P090, diode set : LTC100-B*). The wavelength used for the experiment is 785nm.



Figure 12: The laser diode and its set consisting of the current and temperature controllers, the diode mount and the necessary accessories. © Thorlabs [1]

Beam Shaping Optics:

The radiation from the source is passed through the beam shaping optical components to focus the beam at the sample. The beam diameter on the sample is approximately 1mm. The components for the beam shaping include an aspheric lens, an anamorphic prism pair and a focusing lens. The aspheric lens (*Thorlabs, SITM09*) is used as the collimator just after the laser diode. The anamorphic prism pair (*Thorlabs, PS875-B-N-SF11 Mounted Prism Pair, ARC:650-1050nm, Mag: 2.0*) is put next to the collimator to make the beam spherical in shape because the shape of the beam from a laser diode is always elliptical. Then, a focusing lens (*Thorlabs, AC254-080-B-ML*), which has a focal length 8cm, is used to focus the beam on the phantom.



Figure 13: The beam shaping optical components used in the experiment - a) Collimator , b) Focusing lens and c) Anamorphic Prism Pair. © Thorlabs[1]

Galvo Mirror Set

A galvo mirror pair (*Thorlabs, GVS002*) is used to scan the light source over the sample and direct it towards the required position. It is a 2-dimensional galvo system having two silver coated mirrors with which we can control both the x and y axis in the plane and thus direct the beam accordingly.



Figure 14: The Galvo mirror used to set the direction of the beam. © Thorlabs[1]

Sample

The experiment is carried out in tissue-mimicking solid phantoms which have similar absorption and scattering properties as the tissues[33]. Figure 15 shows a laser beam directed towards such a tissue mimicking phantom. It is seen that the light from the laser gets scattered as well as absorbed inside the phantom in the same way as it happens in tissues.

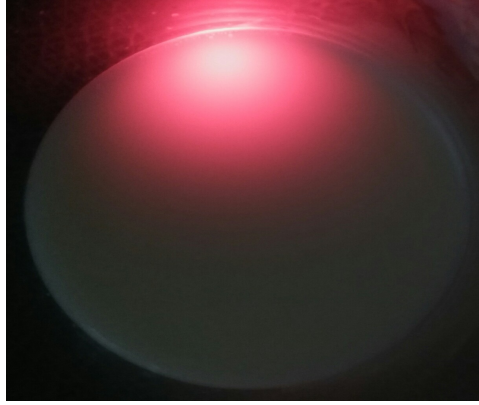


Figure 15: Laser source directed towards a tissue mimicking phantom which shows similar absorption and scattering properties as biological samples.

These phantoms were prepared by us in the laboratory using the standard protocol[34]. As shown in figure 16, a cubical inhomogeneity of approximate size 3mm x 3mm x3mm was introduced inside the phantom at a depth of approximately 3mm from the surface. For more details, check section 2.3.2.

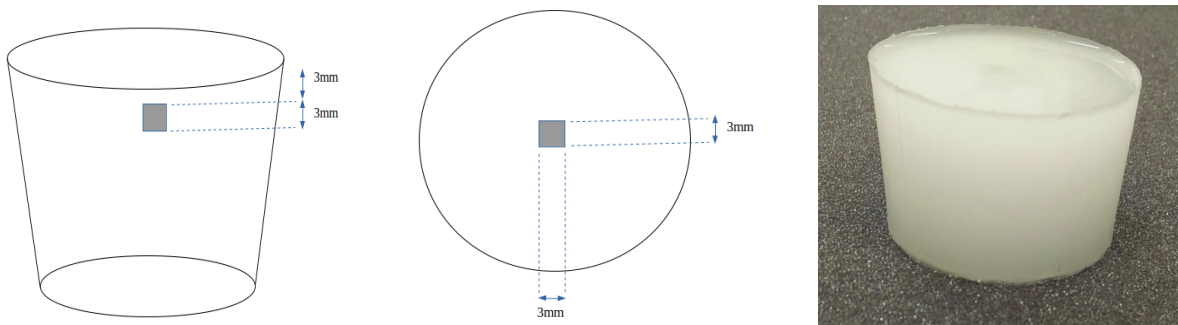


Figure 16: The solid phantom prepared for the experiment and its schematic diagram.

Detector

In the experiment, a CCD camera (Basler, acA640-120um) is used as the detector. It has a resolution of 659 px x 494 px having pixel size of $5.6 \mu\text{m} \times 5.6 \mu\text{m}$ and frame rate of 120 fps.



Figure 17: The CCD camera from Basler used as detector. © Basler [2]

2.3.2 Preparation of Tissue Mimicking Phantoms

The solid tissue-mimicking phantoms used in the experiment were prepared using the standard protocols[34]. The materials used for the preparation include Slygard 184 (PDMS), Sly-

gard 184 Curing Agent and Titanium Dioxide (TiO_2). These are taken in the standard amounts to obtain an absorption coefficient, $\mu_a = 0.021\text{cm}^{-1}$ and a scattering coefficient, $\mu'_s = 8\text{ cm}^{-1}$. For the inhomogeneity, a small amount of Indian Ink (Daler-Rowney Ltd, England) is added to the mixture because this increases its absorption coefficient. Due to the limitations of the detector used in the experiment (CCD camera), the contrast (perturbation in μ_a) of the inhomogeneity is taken higher than the typical values expected in tissue during tumors. If a better detector is used, inhomogeneities with even small contrasts can also be detected successfully.

2.3.3 Experimental Setup

Light from the laser diode passes through the beam shaping optical components which consists of the collimator lens for making the beam parallel; the anamorphic prism for making the cross-sectional shape of the beam circular (because the shape of the beam from a laser diode is always elliptical); and the focusing lens for focusing the beam at the sample. A galvo mirror pair is kept on the path of the beam to direct the beam according to our required direction. The beam hits the sample at the desired position and the images are taken by a CCD camera. Here, figure 18 shows the experimental setup.

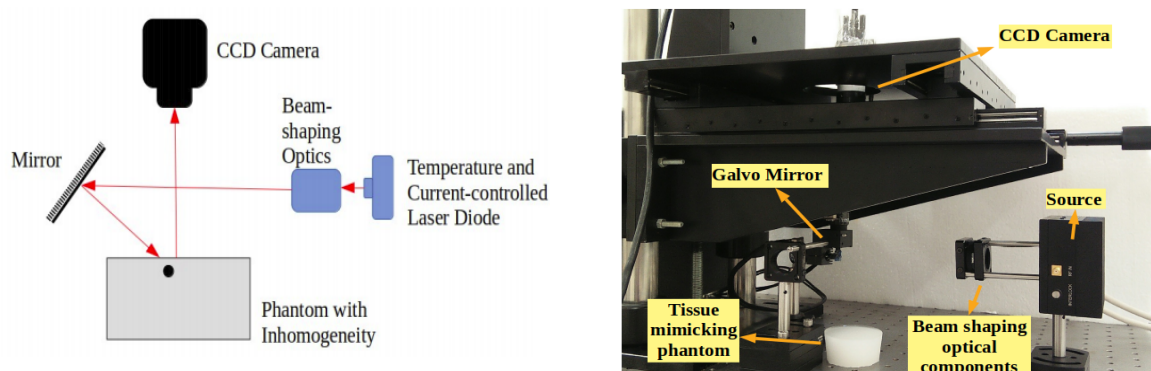


Figure 18: The setup for the experiment - (a) the schematic diagram and (b) the photograph of the setup.

For taking the measurements, a small window (region of interest) of size 1.4cm x 1.1 cm was considered on the surface of the sample as shown in figure 19. In this window, nine pairs of source positions were defined. For each pair, the source is directed such that the highest intensity pixel is seen at the left corner of the image in the first set and at the right corner for the second set. The fluence rates are detected by the CCD camera in array format (each pixel as a detector) for all source positions. All pairs are considered as two-dimensional samples for calculation purposes and thus, calculations are done independently for each pair. We took 500 images for each source position so that the intensity per pixel can later be averaged over all the images of the set to reduce error due to noise. The exposure time for the camera is set at 5ms. We also took corresponding dark images to remove the error due to background light.

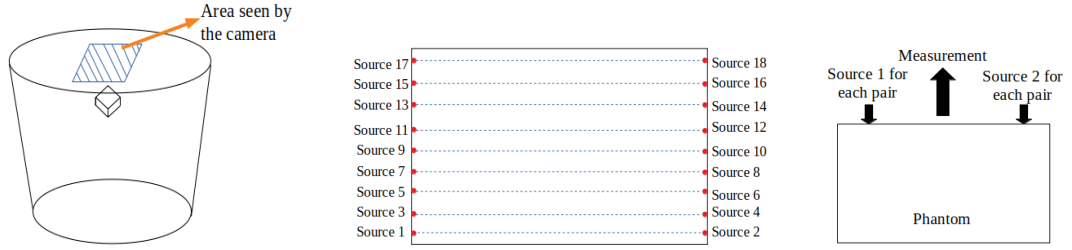


Figure 19: The experimental arrangements for taking the measurements in the phantom.

We plotted the two-dimensional Jacobian combination for each pair and tried to find out the position of the inhomogeneity in that two-dimensional plane. In this way, we can find the approximate location of the inhomogeneity in the sample at different locations, and thus, get a three-dimensional overview. Since, we worked only with simple cases where the inhomogeneity has a constant absorption coefficient throughout, we were also able to calculate the change in absorption coefficient value in the inhomogeneity with respect to the rest of the sample by our method.

3 Results and Discussion

3.1 Results

3.1.1 Simulation Results

We generated a two-dimensional FEM mesh of size 3.8cm x 2.3cm for the simulations as shown in figure 20(a). It has 411 nodes, 68 edges and 752 elements. An inhomogeneity in the absorption coefficient is defined at the position $1.9 < x < 2.4$ and $1.6 < y < 1.8$ as shown in the figure 20(b). The absorption coefficient is taken to be 0.1cm^{-1} for the sample and it is defined as 0.5cm^{-1} in the region of the inhomogeneity.

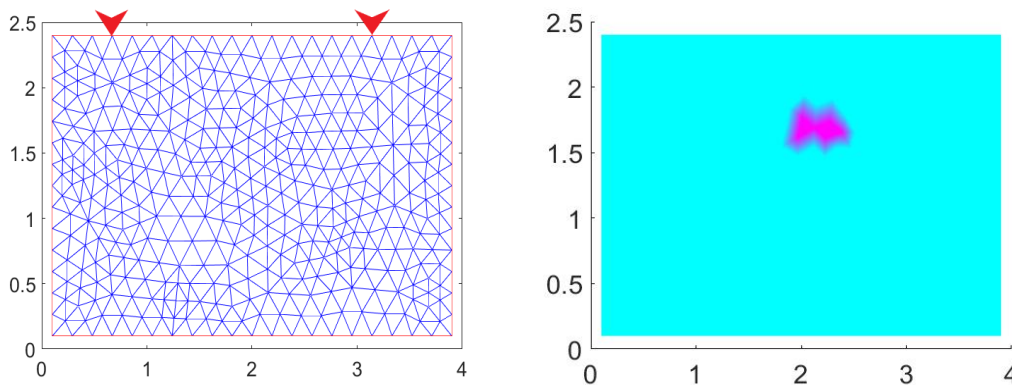


Figure 20: (a) The FEM mesh of side 3.8cm x 2.3 cm used for the simulations ; (b) the inhomogeneity in absorption coefficient introduced in the mesh.

We defined the source positions in the nodes marked by the red arrows as shown in figure 20(a) . In between these two sources, 13 detector nodes were defined for each source. First,

one of the sources is considered and the fluence rate is measured at all the detector nodes by the forward model using the diffusion equation for semi-infinite medium. So, the measurement is obtained as an array of size 13. The same is repeated for the other source and the measurements are obtained for the other source too. Thus, we have two arrays of measurements of size 13 each for the sample. Next, we need to find the combination of fluence rates.

All the combinations of the measurements are calculated by multiplication of fluence rate value for one source with that for the other source. So, a square matrix of size 13 x 13 is obtained. In figure 21, the vertical axis in the matrix corresponds to the detectors for the first source and the horizontal axis corresponds to the detectors for the second source. (All the detectors were labelled from left to right in the simulations.) In figure 21, it is seen that the product values are highest for the combination of fluence rates for detector 1 for source 1 and detector 13 for source 2. This is because detector 1 is nearest to source 1 and detector 13 is nearest to source 2. So, their combination gives the highest value. Also, the inhomogeneity do not lie on the path of their Jacobians. It is also observed that the product value decreases as we move away from the source. This is because as the distance from the source increases, the measurement values drops exponentially as shown in figure 2.

The same procedure of calculation of square matrix of size 13x13 was carried out for the baseline where the medium is considered to be homogenous with an absorption coefficient of 0.1cm^{-1} . The calculated matrix is shown in figure 22. A same trend as figure 21 is seen in the baseline case too.

We want to see the change in the measurement values due to the presence of the inhomogeneity with respect to the baseline. So, we subtract the matrix shown in figure 21 from the matrix for the baseline shown in figure 22, and find the percentage change in each value of the matrix. The matrix obtained by doing so is shown in figure 23. It is seen that there are certain values in the matrix in figure 23 which are much higher, while there are certain values which are almost negligible. This means the inhomogeneity must be in the path of the Jacobian combinations for these detector pairs which show a high change in the values. We took a thresholding

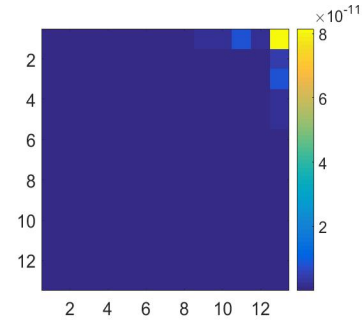


Figure 21: The matrix showing the values of the product of measurements due to the two sources for the sample with inhomogeneity.

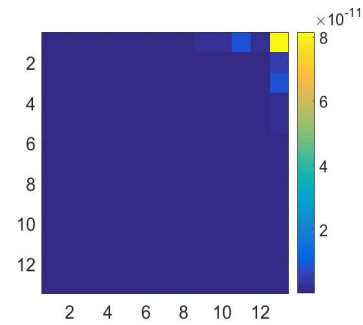


Figure 22: The matrix showing the values of the product of measurements due to the two sources for the baseline.

of top 96% of the maximum change value and thus, pick all the detector pairs which has change values higher than 96% of the maximum change. When we plot the combination Jacobian for all the pairs of detectors for the two sources which are higher than the threshold value, it gives the approximate position of the inhomogeneity.

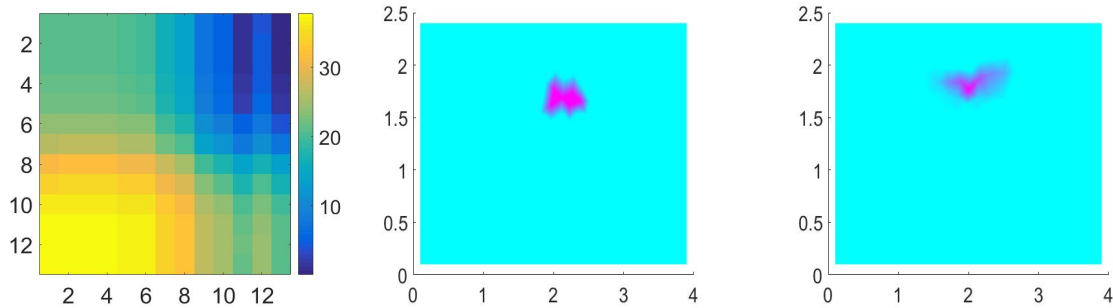


Figure 23: (a)The matrix showing the percentage change in values of the matrix with respect to the baseline; (b) the position of the inhomogeneity in the sample as shown by the highlighted region; (c) the Jacobian combination showing the detected position of the inhomogeneity.

Thus, we can find the approximate position of the inhomogeneity by this method of combination of Jacobians. We can also find the approximate change in absorption coefficient without inversion of the Jacobian matrix as described in last part of section 2.1 by equation (18). For the inhomogeneity defined by us with a change in absorption coefficient is 0.4cm^{-1} (0.5cm^{-1} for inhomogeneity and 0.1cm^{-1} for the rest of the sample), the calculated change in absorption coefficient is $3.88 \times 10^{-2}\text{cm}^{-1}$. It is observed that the calculated change is less than the given change by an order of 10 approximately.

We tried to calculate the change in absorption coefficients by assigning different values of absorption coefficient to the inhomogeneity. This is shown in table 1.

Table 1: The given and the calculated values of μ_a^δ for the inhomogeneity in the sample.

Given μ_a^δ value (cm^{-1})	Calculated μ_a^δ value (cm^{-1})
4.00×10^{-3}	4.84×10^{-4}
1.00×10^{-2}	1.20×10^{-3}
1.00×10^{-1}	1.14×10^{-2}
2.00×10^{-1}	2.16×10^{-2}
3.00×10^{-1}	3.07×10^{-2}
4.00×10^{-1}	3.88×10^{-2}

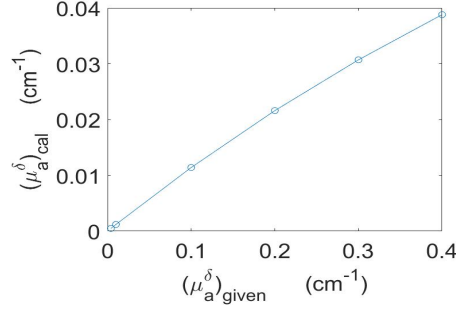


Figure 24: A graph showing the given versus the calculated values of μ_a^δ for the inhomogeneity in the sample.

It is seen in table 1 that the ratio at which the given values of μ_a^δ is changing is almost being maintained in the calculated values too. But all the calculated values are less than the given values by a factor of 10 approximately. We can consider this as a calibration factor for the calculations. Thus, taking 10 as a calibration factor and multiplying all the calculated values by 10, we get the following values of μ_a^δ as shown in table 2. This is very close to the given values of μ_a^δ .

Table 2: The given and the calculated values of μ_a^δ for the inhomogeneity in the sample after multiplying the calculated values by the calibration factor 10.

Given μ_a^δ value (cm ⁻¹)	Calculated μ_a^δ value (cm ⁻¹)
4.00×10^{-3}	4.84×10^{-3}
1.00×10^{-2}	1.20×10^{-2}
1.00×10^{-1}	1.14×10^{-1}
2.00×10^{-1}	2.16×10^{-1}
3.00×10^{-1}	3.07×10^{-1}
4.00×10^{-1}	3.88×10^{-1}

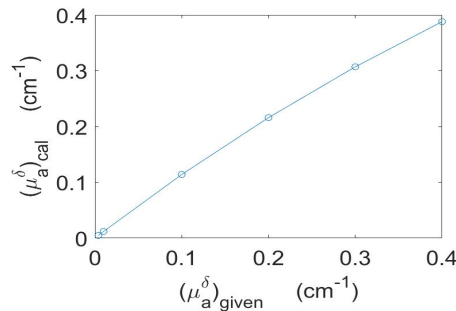


Figure 25: A graph showing the given versus the calculated values of μ_a^δ for the inhomogeneity in the sample after multiplying the calculated values with the calibration factor.

Next, we tried to compare our method with the existing methods which are commonly used for the detection of inhomogeneity in a biological sample. For most cases, the diffusion equation is directly solved by inverting the Jacobian matrix using the method of Tikhonov regularization. Equation (12) shows the inversion of the Jacobian matrix using this method. We tried

to reconstruct the same inhomogeneity shown in figure 20 by using the same FEM mesh by Tikhonov regularization so that we can have a direct comparison. The reconstructed image is shown in figure 26.

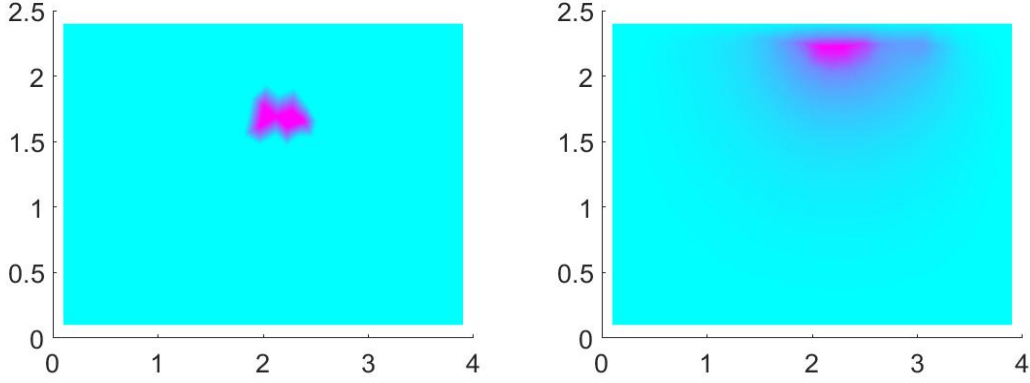


Figure 26: (a)The position of the inhomogeneity as shown by the highlighted region;(b) the inhomogeneity reconstructed by inversion of the Jacobian matrix by using Tikhonov regularization.

In figure 26, it is seen that the position of the inhomogeneity in the reconstructed image is shifted towards the superficial layers of the sample. This is expected because of the properties of the Jacobian matrix. So, to address this problem, depth compensation algorithms are generally incorporated along with the Tikhonov regularization to locate the inhomogeneity in a better way. In equation (13), a depth compensation algorithm has been used for this purpose. So, we shall reconstruct the inhomogeneity by using this equation and try to compare the result with our proposed method.

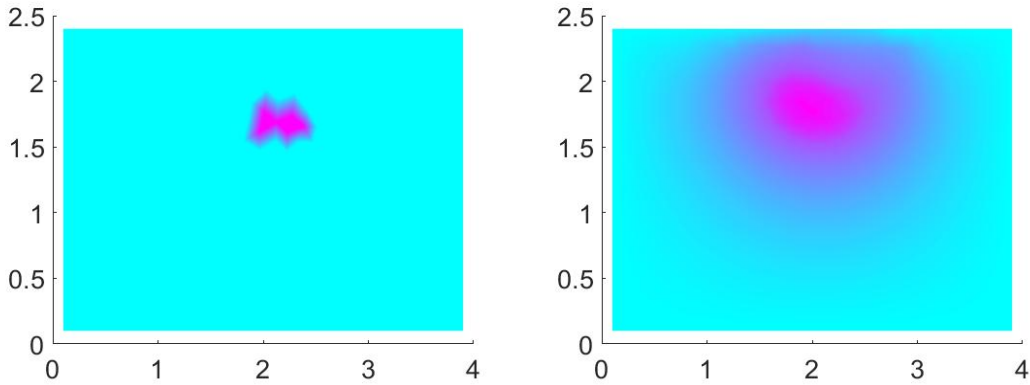


Figure 27: (a)The position of the inhomogeneity as shown by the highlighted region;(b) the inhomogeneity reconstructed by using depth compensation algorithm.

Figure 27 shows the reconstructed image of the sample after using an appropriate depth-compensation algorithm. It is observed that in this reconstructed image, the inhomogeneity is not shifted towards the surface layers. However, the location of the inhomogeneity is not precisely shown by this method. Apart from that, the main difficulty of using such inversion methods for reconstruction is the presence of the regularization constants λ_1 and λ_2 which are

difficult to determine. In fact, there is always a possibility to get a better reconstruction of the sample by using a better values of these regularization constants.

In our proposed Jacobian combination method, no such parameters are being used. So, this makes the computation using this method more easier. All these reasons makes the Jacobian combination method a simpler way of locating the inhomogeneity.

3.1.2 Experimental Results

As shown in figure 19, a region of interest of size 1.4cm x 1.1 cm was considered on the surface of the sample where nine pairs of source positions were taken. For each source, the fluence rates were detected by the CCD camera in array format (each pixel as a detector). The matrices are calculated by multiplying the fluence rates detected by the detector array for the two sources independently and thus, the change matrices are calculated with respect to the baseline. In the change matrix, thresholding is being set at top 96% of the maximum value of change. So, Jacobians are being plotted for all those pairs of source-detectors which had change more than 96% of the maximum change value in the change matrix.

For plotting the Jacobians, an FEM mesh was constructed of size 1.8cm x 1.3cm as shown in figure 28, having 8217 nodes, 16128 elements and 304 edges. In this mesh, the two source positions are defined on the top surface of the mesh such that the distance between them is approximately 1.4cm, same as our experimental case. The measurements at all detector positions are also being interpolated to the mesh.

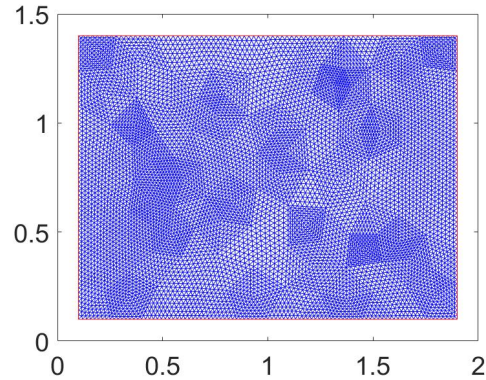


Figure 28: The FEM mesh constructed to plot the Jacobians for the experiment.

It was observed that out of nine pairs, only six pairs had high change in the product of fluence rate values compared to the baseline. The rest three pairs had almost negligible change. So, this means that six pairs of detector were in the region of inhomogeneity and the other three pairs did not have the inhomogeneity below them. The Jacobians are being plotted for these six pairs which had the inhomogeneity below them and these are shown in figure 29. From these figures, the location of the inhomogeneity is being determined. It is observed that the location detected by our method is similar to the location of the inhomogeneity defined by us which is shown in figure 30. The inhomogeneity is seen at a depth of approximately 3mm in the detected location as expected.

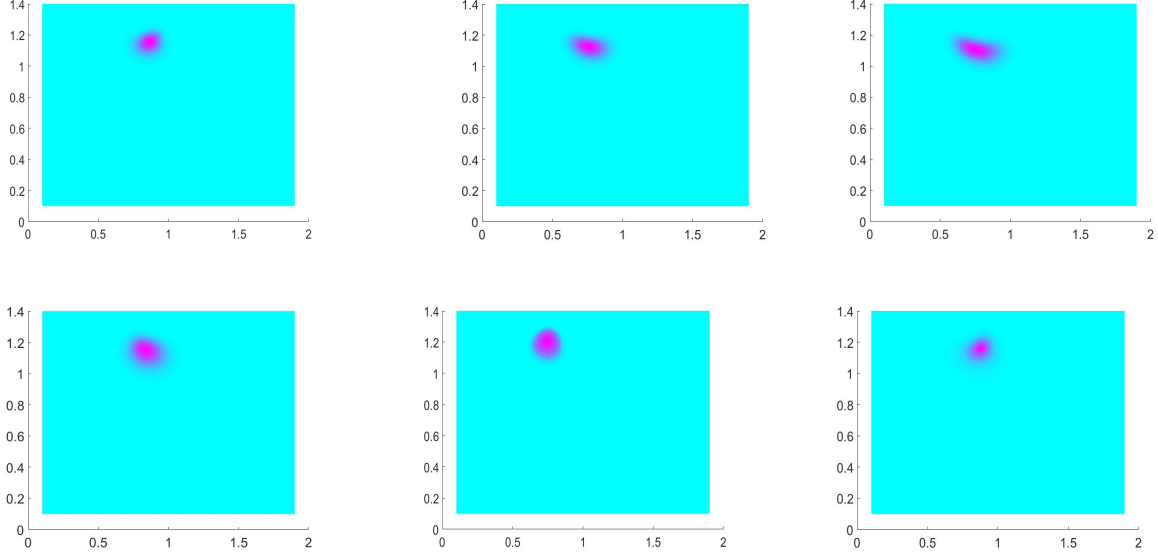


Figure 29: The position of the inhomogeneity as seen by detector arrays located between the source pairs.

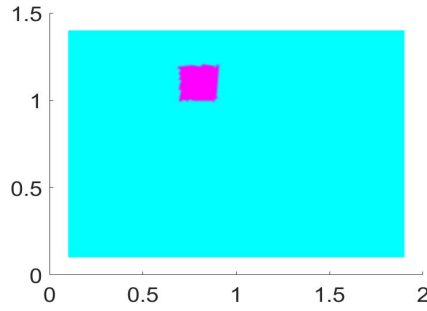


Figure 30: Position of the inhomogeneity as defined by us in the phantom.

We also quantified the value of change in absorption coefficient for each pair independently by using our method. These are shown in table 3. We have multiplied the calculated μ_a^δ value by the calibration factor 10 to obtain these values. For all the layers, the value is approximately same which was expected.

Table 3: The calculated values of μ_a^δ for the inhomogeneity in the experiment after multiplying them by the calibration factor 10.

Source pair	Calculated μ_a^δ (cm^{-1})	Mean μ_a^δ (cm^{-1})
Source 1-Source 2	2.77	2.66
Source 3-Source 4	2.45	
Source 5-Source 6	2.81	
Source 7-Source 8	2.61	
Source 9-Source 10	2.87	
Source 11-Source 12	2.47	

The calculated μ_a^δ for our experimental case is approximately 2.66 cm^{-1} .

3.2 Discussion

As per our hypothesis, we are able to detect any inhomogeneity present in a biological sample by using the properties of the Jacobians associated with the source and detector pairs defined on the sample surface. We carried out simulations as well as experiments to prove our hypothesis. This method is also expected to work if we perturbed the scattering coefficient instead to the absorption coefficient in the region of inhomogeneity in the sample.

The simulations were done for two-dimensional case using FEM mesh in the Matlab software. An inhomogeneity was introduced at a particular depth in the sample and we tried to detect it using our proposed method. We were able to detect the approximate position by combining all the Jacobians for those source-detector pairs whose measurements got highly affected due to the presence of the inhomogeneity in the sample. This is shown in figure 23 for the simulation case. We also successfully quantified the perturbation in the absorption coefficient in the sample for simple cases where the absorption coefficient was constant throughout the inhomogeneity region. It was seen that we can detect even the smallest change in the absorption coefficient which is shown in table 2. However, for practical cases, due to the limitations set by noise, this may not be possible.

The experiments are carried out in tissue-mimicking phantoms which are prepared such that they have the same absorption and scattering properties as tissues. For the inhomogeneity, Indian ink was added during preparation for increasing its absorption coefficient with respect to the rest of the sample. It was introduced at a particular depth inside the phantom. The experimental setup was set as shown in figure 18 for detection of the inhomogeneity. We selected a region of interest of size 1.4cm x 1.1 cm in the sample surface and nine pairs of source positions were defined in that area. All the calculations were done independently for all nine pairs by considering them as independent 2-dimensional setups.

4 Conclusions and Outlook

In this thesis, we presented a new method for detection and positioning an inhomogeneity present in any biological sample having the typical absorption and scattering properties. We were also able to quantify the change in properties of the sample in the inhomogeneity region for simple cases. This method is expected to reduce the computational load and also reconstruct the details in the sample in a more precise way compared to the pre-existing methods. We proved our hypothesis in simulations and also in experiments. All the computational work is done using the Matlab software. The simulations were carried out using the Finite Element Method (FEM). The experiment was done in tissue-mimicking phantoms prepared in the laboratory which possess the same absorption and scattering properties as tissues.

In the experiment, the inhomogeneity present in the sample, which is being reconstructed, had very high contrast with respect to the background. We used such a sample for the experiment because of the limitations of the detection system. By using a detector with better specifications, very small contrast in the inhomogeneity can also be reconstructed by our method.

This method seems to be very promising and this can have many applications in the medical field. It can be used for detection of tumor in brain or breast in future.

A Appendix I : Important Definitions

Radiance:

Radiance is defined as the flow of energy per unit solid angle per unit normal area and per unit time over a narrow range of frequency. Radiance at position \vec{r} in the direction \hat{s} and at time t is denoted by $L(\vec{r}, \hat{s}, t)$. Its unit is $\text{Wm}^{-2}\text{sr}^{-1}$ [22].

Fluence Rate:

The radiance averaged over all the directions without taking the direction into consideration for a particular distance $|\vec{r}|$ is known as fluence rate for that distance and at time t [22]. It is a scalar quantity and its unit is Wm^{-2} . It is given by:

$$\Phi(\vec{r}, t) = \int_{4\pi} L(\vec{r}, \hat{s}, t) d\Omega$$

Current Density:

The radiance averaged over all the directions by taking account of the direction for a particular distance $|\vec{r}|$ is known as current density for that distance and at time t [22]. It is a vector quantity and its unit is Wm^{-2} . It is given by:

$$\vec{J}(\vec{r}, t) = \int_{4\pi} \hat{s} L(\vec{r}, \hat{s}, t) d\Omega$$

Scattering Length:

When photon travels through a scattering medium, the distance travelled by it before it gets scattered is known as scattering length [21]. It has unit of length.

Trnsport Mean Free Path:

When photon travels through a scattering medium, the direction of the photon gets randomized after a particular distance. This distance is defined as transport mean free path [21]. It has unit of length.

Absorption Length:

When photon travels through a absorbing medium, the distance travelled by it before it gets completely absorbed is known as absorption length [21]. It has unit of length.

Scattering Coefficient:

Scattering coefficient is defined as the reciprocal of scattering length [21]. It has unit of inverse of length. It is denoted by μ_s .

Reduced Scattering Coefficient:

The reduced scattering length is the reciprocal of transport mean free path [21]. It is denoted by μ'_s has unit of inverse of length. It is related to the scattering coefficient μ_s by the relation [22],

$$\mu'_s = \mu_s(1 - g)$$

where g is known as the anisotropy factor which gives the measure of the change in direction experienced by a photon after a single scattering event. Typically, it has value 0.9 (approx.) for tissue [20].

Absorption Coefficient:

The reciprocal of absorption length is defined as absorption coefficient [21]. It has unit of inverse of length and its denoted by μ_a .

References

- [1] Thorlabs. <http://https://www.thorlabs.com/>. [seen on 10th March, 2019].
- [2] Basler. <https://www.baslerweb.com/>. [seen on 10th March, 2019].
- [3] Frans F Jobsis. Noninvasive, infrared monitoring of cerebral and myocardial oxygen sufficiency and circulatory parameters. *Science*, 198(4323):1264–1267, 1977.
- [4] Frans F Jobsis-vander Vliet. Discovery of the near-infrared window into the body and the early development of near-infrared spectroscopy. *Journal of biomedical optics*, 4(4):392–397, 1999.
- [5] Marco Ferrari and Valentina Quaresima. A brief review on the history of human functional near-infrared spectroscopy (fnirs) development and fields of application. *Neuroimage*, 63(2):921–935, 2012.
- [6] Gemma Bale, Clare E Elwell, and Ilias Tachtsidis. From jöbssis to the present day: a review of clinical near-infrared spectroscopy measurements of cerebral cytochrome-c-oxidase. *Journal of biomedical optics*, 21(9):091307, 2016.
- [7] Arjun Yodh and Britton Chance. Spectroscopy and imaging with diffusing light. *Physics Today*, 48(3):34–41, 1995.
- [8] Regine Choe. *Diffuse optical tomography and spectroscopy of breast cancer and fetal brain*. Citeseer, 2005.
- [9] Turgut Durduran, Regine Choe, Guoqiang Yu, Chao Zhou, Julia C Tchou, Brian J Czerniecki, and Arjun G Yodh. Diffuse optical measurement of blood flow in breast tumors. *Optics letters*, 30(21):2915–2917, 2005.
- [10] Chao Zhou, Regine Choe, Natasha S Shah, Turgut Durduran, Guoqiang Yu, Amanda Durkin, David Hsiang, Rita Mehta, John A Butler, Albert E Cerussi, et al. Diffuse optical monitoring of blood flow and oxygenation in human breast cancer during early stages of neoadjuvant chemotherapy. *Journal of biomedical optics*, 12(5):051903, 2007.
- [11] Jeremy C Hebden and Topun Austin. Optical tomography of the neonatal brain. *European radiology*, 17(11):2926, 2007.
- [12] M Cope and David T Delpy. System for long-term measurement of cerebral blood and tissue oxygenation on newborn infants by near infra-red transillumination. *Medical and Biological Engineering and Computing*, 26(3):289–294, 1988.

- [13] Jane E Brazy, Darrell V Lewis, Michael H Mitnick, and Frans F Jöbsis vander Vliet. Non-invasive monitoring of cerebral oxygenation in preterm infants: preliminary observations. *Pediatrics*, 75(2):217–225, 1985.
- [14] JS Wyatt, DT Delpy, M Cope, Susan Wray, and EOR Reynolds. Quantification of cerebral oxygenation and haemodynamics in sick newborn infants by near infrared spectrophotometry. *The Lancet*, 328(8515):1063–1066, 1986.
- [15] Meeri N Kim, Turgut Durduran, Suzanne Frangos, Brian L Edlow, Erin M Buckley, Heather E Moss, Chao Zhou, Guoqiang Yu, Regine Choe, Eileen Maloney-Wilensky, et al. Noninvasive measurement of cerebral blood flow and blood oxygenation using near-infrared and diffuse correlation spectroscopies in critically brain-injured adults. *Neurocritical care*, 12(2):173–180, 2010.
- [16] Turgut Durduran, Chao Zhou, Erin M Buckley, Meeri N Kim, Guoqiang Yu, Regine Choe, J William Gaynor, Thomas L Spray, Suzanne M Durning, Stefanie E Mason, et al. Optical measurement of cerebral hemodynamics and oxygen metabolism in neonates with congenital heart defects. *Journal of biomedical optics*, 15(3):037004, 2010.
- [17] Chao Zhou, Stephanie A Eucker, Turgut Durduran, Guoqiang Yu, Jill Ralston, Stuart H Friess, Rebecca N Ichord, Susan S Margulies, and Arjun G Yodh. Diffuse optical monitoring of hemodynamic changes in piglet brain with closed head injury. *Journal of biomedical optics*, 14(3):034015, 2009.
- [18] Chao Zhou, Tomokazu Shimazu, Turgut Durduran, Janos Luckl, Daniel Y Kimberg, Guoqiang Yu, Xiao-Han Chen, John A Detre, Arjun G Yodh, and Joel H Greenberg. Acute functional recovery of cerebral blood flow after forebrain ischemia in rat. *Journal of Cerebral Blood Flow & Metabolism*, 28(7):1275–1284, 2008.
- [19] Turgut Durduran, Chao Zhou, Brian L Edlow, Guoqiang Yu, Regine Choe, Meeri N Kim, Brett L Cucchiara, Mary E Putt, Qaisar Shah, Scott E Kasner, et al. Transcranial optical monitoring of cerebrovascular hemodynamics in acute stroke patients. *Optics express*, 17(5):3884–3902, 2009.
- [20] Wai-Fung Cheong, Scott A Prahl, and Ashley J Welch. A review of the optical properties of biological tissues. *IEEE journal of quantum electronics*, 26(12):2166–2185, 1990.
- [21] Turgut Durduran, Regine Choe, Wesley B Baker, and Arjun G Yodh. Diffuse optics for tissue monitoring and tomography. *Reports on Progress in Physics*, 73(7):076701, 2010.
- [22] Lihong V Wang and Hsin-i Wu. *Biomedical optics: principles and imaging*. John Wiley & Sons, 2012.
- [23] Subrahmanyan Chandrasekhar. *Radiative transfer*. Courier Corporation, 2013.

- [24] Daniele Contini, Fabrizio Martelli, and Giovanni Zaccanti. Photon migration through a turbid slab described by a model based on diffusion approximation. i. theory. *Applied optics*, 36(19):4587–4599, 1997.
- [25] V Venugopalan, JS You, and BJ Tromberg. Radiative transport in the diffusion approximation: an extension for highly absorbing media and small source-detector separations. *Physical Review E*, 58(2):2395, 1998.
- [26] Michael I Mishchenko. Radiative transfer theory: From maxwell’s equations to practical applications. In *Wave Scattering in Complex Media: From Theory to Applications*, pages 366–414. Springer, 2003.
- [27] Michael I Mishchenko. Maxwell’s equations, radiative transfer, and coherent backscattering: A general perspective. *Journal of Quantitative Spectroscopy and Radiative Transfer*, 101(3):540–555, 2006.
- [28] Simon R Arridge and John C Schotland. Optical tomography: forward and inverse problems. *Inverse Problems*, 25(12):123010, 2009.
- [29] Mario Bertero and Patrizia Boccacci. *Introduction to inverse problems in imaging*. CRC press, 1998.
- [30] Brian White. Developing high-density diffuse optical tomography for neuroimaging. 2012.
- [31] Martin Schweiger, Simon R Arridge, and David T Delpy. Application of the finite-element method for the forward and inverse models in optical tomography. *Journal of Mathematical Imaging and Vision*, 3(3):263–283, 1993.
- [32] Martin Schweiger, SR Arridge, M Hiraoka, and DT Delpy. The finite element method for the propagation of light in scattering media: boundary and source conditions. *Medical physics*, 22(11):1779–1792, 1995.
- [33] Rinaldo Cubeddu, Antonio Pifferi, Paola Taroni, Alessandro Torricelli, and Gianluca Valentini. A solid tissue phantom for photon migration studies. *Physics in Medicine & Biology*, 42(10):1971, 1997.
- [34] Frederick Ayers, Alex Grant, Danny Kuo, David J Cuccia, and Anthony J Durkin. Fabrication and characterization of silicone-based tissue phantoms with tunable optical properties in the visible and near infrared domain. In *Design and Performance Validation of Phantoms Used in Conjunction with Optical Measurements of Tissue*, volume 6870, page 687007. International Society for Optics and Photonics, 2008.